

This is an Open Access document downloaded from ORCA, Cardiff University's institutional repository: <https://orca.cardiff.ac.uk/id/eprint/111814/>

This is the author's version of a work that was submitted to / accepted for publication.

Citation for final published version:

Han, Yu, Li, Qiang , Ng, Kar Wei, Zhu, Si and Lau, Kei May 2018. InGaAs/InP quantum wires grown on silicon with adjustable emission wavelength at telecom bands. *Nanotechnology* 29 (22) , 225601. 10.1088/1361-6528/aab53b

Publishers page: <http://dx.doi.org/10.1088/1361-6528/aab53b>

Please note:

Changes made as a result of publishing processes such as copy-editing, formatting and page numbers may not be reflected in this version. For the definitive version of this publication, please refer to the published source. You are advised to consult the publisher's version if you wish to cite this paper.

This version is being made available in accordance with publisher policies. See <http://orca.cf.ac.uk/policies.html> for usage policies. Copyright and moral rights for publications made available in ORCA are retained by the copyright holders.



InGaAs/InP quantum wires grown on silicon with adjustable emission wavelength at telecom bands

Yu Han¹, Qiang Li¹, Kar Wei Ng², Si Zhu¹ and Kei May Lau^{1, a)}

1 Department of Electronic and Computer Engineering, Hong Kong University of Science and Technology, Clear Water Bay, Kowloon, Hong Kong

2 Institute of Applied Physics and Materials Engineering, University of Macau, Avenida da Universidade, Macau

^{a)} Tel: (852)23587049, Fax: (852) 23581485, Email: EEKMLAU@UST.HK

Abstract

We report the growth of vertically stacked InGaAs/InP quantum wires on (001) Si substrates with adjustable room-temperature emission at telecom bands. Based on a self-limiting growth mode in selective area metal-organic chemical vapor deposition, crescent-shaped InGaAs quantum wires with variable dimensions are embedded within InP nano-ridges. With extensive transmission electron microscopy studies, the growth transition and morphology change from quantum wires to ridge quantum wells have been revealed. As a result, we are able to decouple the quantum wires from ridge quantum wells and manipulate their dimensions by scaling the growth time. With minimized lateral dimension and their unique positioning, the InGaAs/InP quantum wires are more immune to dislocations and more efficient in radiative processes, as evidenced by their excellent optical quality at telecom-bands. These promising results thus highlight the potential of combining low-dimensional quantum wire structures with the aspect ratio trapping process for integrating III-V nano-light emitters on mainstream (001) Si substrates.

Introduction

Integration of optical links with Si-based electronics holds great promise to overcome the inter/intra-chip communication bottleneck faced by present microprocessors.^{1,2} To fully exploit the economy of CMOS foundry technologies, monolithic integration of III-V lasers on Si is being extensively researched, taking advantage of the active light emitting property of III-V materials with the passive wave-guiding characteristic of silicon.³⁻⁶ Recent advancements in selective area hetero-epitaxy combined with the aspect ratio trapping (ART) technique have demonstrated proof-of-concept integration schemes with CMOS compatibility.⁷⁻¹⁴ However, it is still unclear if the good crystalline quality enabled by the defect trapping mechanism of ART can sustain high reliability laser operation. Kunert et.al reported large GaAs/InGaAs nano-ridge structures grown out of narrow trenches, which could potentially eliminate all threading dislocations.¹⁵ However, achieving InP/InGaAs nano-ridges using the same approach towards emission at telecom-wavelengths has been hindered by the difficulty in controlling the faceting of InP. We hereby demonstrate an alternative route to minimize the effect of threading dislocations by leveraging low dimensional InGaAs/InP quantum wires (QWRs) grown on V-grooved Si. The nanometer-scale lateral dimension and the unique localization of these QWRs render them almost immune to 60° dislocations. Additionally, compared with quantum wells (QWs),¹⁶⁻²¹ the strong two dimensional quantum confinement associated with QWRs leads to excellent optical property at telecom-bands, as attested by room temperature micro-photoluminescence (μ -PL) measurements. The spiked-shaped density of states (DOS) of the one dimensional QWRs could also potentially benefit nano-laser performance in terms of low threshold and high temperature stability. Through extensive transmission electron microscopy (TEM) investigation, we present the growth mechanism of the

InGaAs QWRs. We also show that, by manipulating the dimension of the InGaAs QWRs, the emission wavelength could be widely adjusted to cover the whole telecommunication band.

Experimental details

The epitaxial growth was performed in a metal-organic chemical vapor deposition (MOCVD) system with a horizontal reactor (AIXTRON 200/4). We adopted a three-step growth procedure, starting with an ultra-thin GaAs stress-relaxing layer, followed by a thin InP nucleation layer and finally a thick InP buffer layer. Details of sample preparation and growth parameters have been reported elsewhere.^{22, 23} Figure 1(a), a top-view scanning electron microscopy (SEM) image of an as-grown sample, reveals a uniform InP nano-ridge array in a large area. The zoomed-in 70° tilted SEM image in figure 1(b) indicates faceted growth, with the top {111}B InP facets mirroring the bottom {111} Si surfaces. The spacing of the InP nano-ridges can be controlled by the separation of the oxide openings (see figure 1(c)) on the patterning mask.

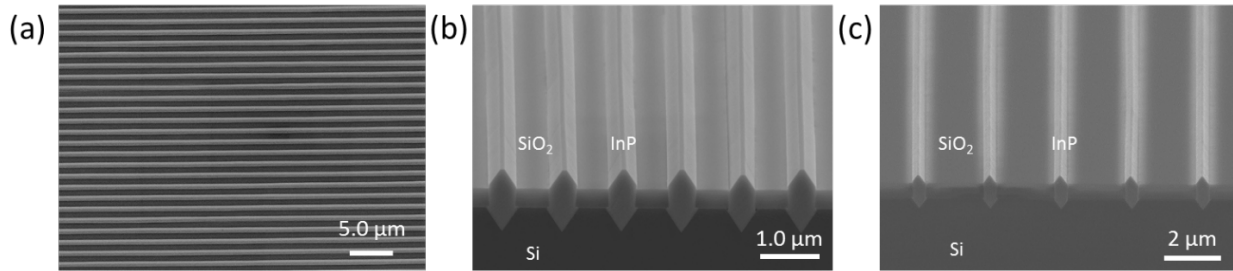


Figure 1. (a) Top-view SEM image of the as-grown in-plane InP nano-ridges on (001) Si. (b) 70° tilted SEM image of the InP nano-ridges with faceted growth front. (c) InP nano-ridge array with larger separations.

The InP nano-ridge and inserted InGaAs QWRs were further investigated using cross-sectional TEM. Figure 2 (a) shows a high-angle annular dark-field scanning transmission electron microscopy (HAADF-STEM) image of a typical InP nano-ridge. Stacked InGaAs QWR structures are clearly identified at the upper part of the InP nano-ridge. The growth time of each QWR was 15 sec in this particular structure. Zoomed-in HAADF-STEM inspection of the top three QWRs suggests a triangular shape with a width of 30 nm and a height of 20 nm (see figure 2(c)). In addition to the QWRs, a 3 nm thick InGaAs QW was also formed along the {111} ridges (figure 2(b)), exhibiting a uniform thickness and a sharp interface between InGaAs and InP. The existence of the ridge QWs, however, is undesirable for efficient light emission since they are more vulnerable to defects propagated from the III-V/Si interfaces. Therefore, it is crucial to eradicate the ridge QWs so as to enhance quantum confinement and minimize carrier escape from the QWRs into the ridge QWs. Figure 2(d) shows a cross-sectional TEM image of four stacked InGaAs QWRs with a growth time of 2.0 sec. Compared with the QWRs with a 15 sec growth time, reducing the InGaAs growth time to 2.0 sec effectively suppresses the formation of ridge QWs. Zoomed-in inspection of the QWR in figure 2(e) suggests a similar wire structure. Further reduction of the growth time to 1.0 sec and 0.5 sec results in the vertical shrinkage of the QWR from 20 nm to 7 nm, and then to 2 nm (figure 2(f) and (g)). The different quantum confinement associated with the varying vertical dimension implicates the tunability of the emission wavelength at telecom bands.

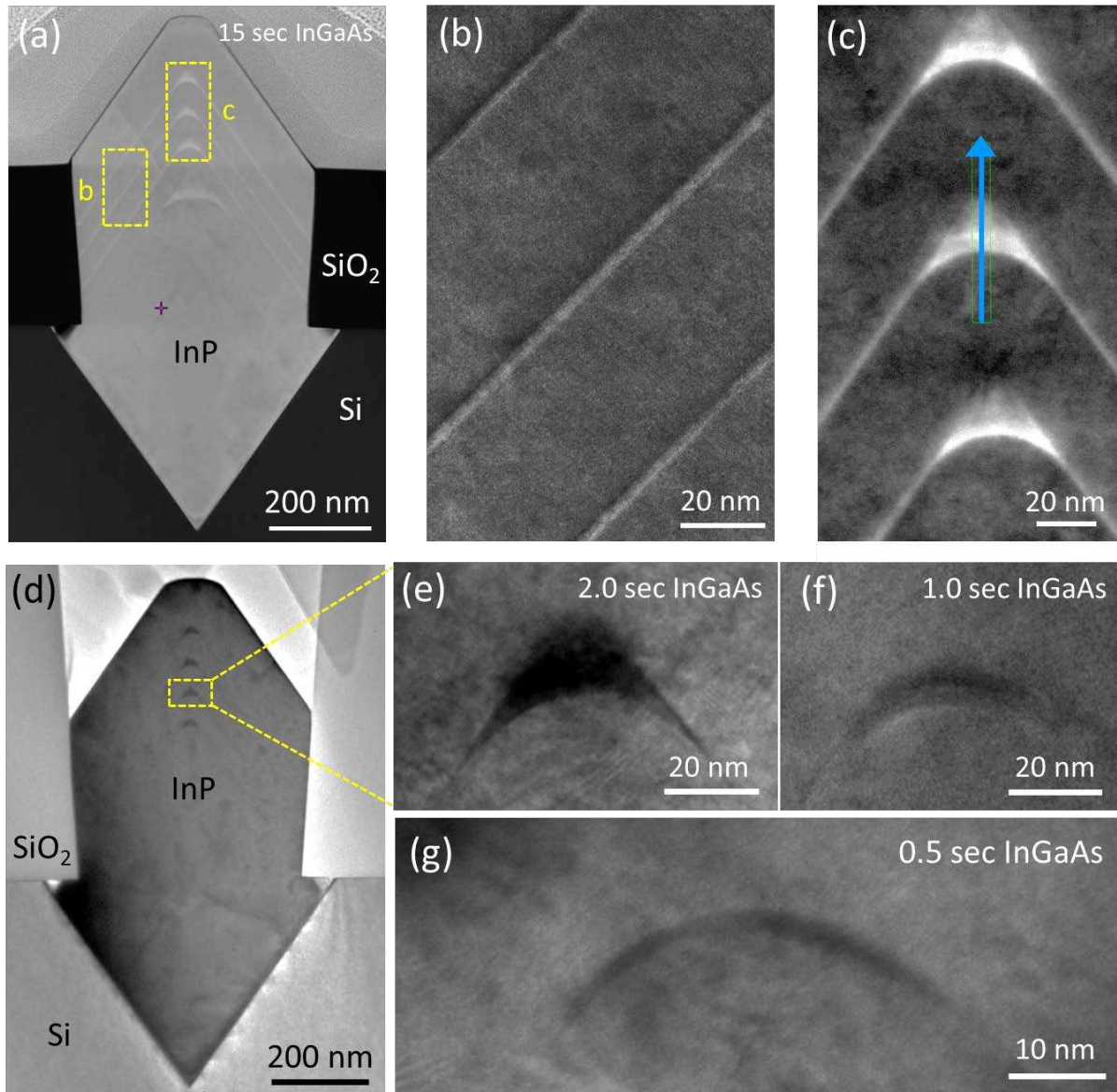


Figure 2. (a) HAADF-STEM image of one representative InP/InGaAs nano-ridge with a InGaAs growth time of 15 sec; Stacked InGaAs QWRs are clearly visible. (b) High resolution TEM image of the {111} InGaAs ridge QWs with sharp InP/InGaAs interfaces; (c) Zoomed-in HAADF-STEM image of the top three InGaAs QWRs. The QWRs exhibit a triangular shape with lateral dimension of 30 nm and vertical dimension of 20 nm. (d) Cross-sectional TEM image of the QWRs with a growth time of 2.0 sec, showing four stacked InGaAs QWRs. (e)-(g) Zoomed-in cross sectional TEM images of InGaAs QWRs with different growth times (2.0 sec, 1.5 sec and 0.5 sec). The vertical size of the QWR reduces as the growth time scales down.

Results and discussion

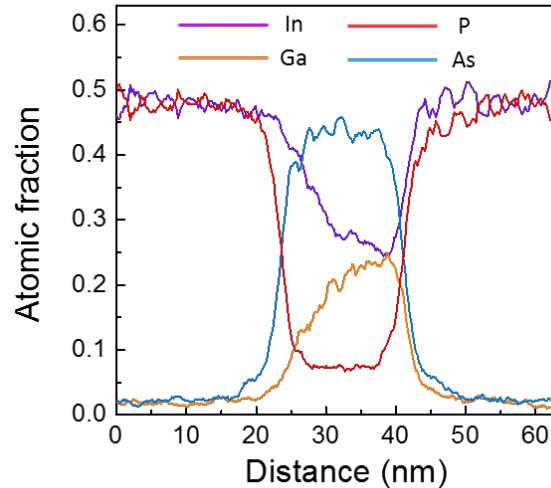


Figure 3. EDS line-scan of one InGaAs QWR, showing composition inhomogeneity along the vertical direction of the QWR. The bottom of the QWR has a higher indium composition while the tip of the QWR has a larger gallium composition.

We then performed energy dispersive spectroscopy (EDS) line-scan of one QWR to study the chemical composition (scanning line shown in figure 2(c)), and summarized the measured results in figure 3. Both the indium and gallium composition show inhomogeneity along the vertical direction of the QWR. The indium composition decreases monotonically from the bottom to the top of the QWR, while the gallium composition shows a reverse trend. This elemental distribution agrees well with the decreasing brightness in the HAADF image of the QWR (brightness of the HAADF image is approximately proportional to the square of the average atomic number). The average indium fraction of the InGaAs is around 0.53 according to the X-ray diffraction measurement of the sample with a thick InGaAs calibration layer. The composition inhomogeneity could be attributed to the difference in the diffusion coefficients of indium and gallium adatoms

along the transitional facets.²⁴ Based on the EDS measurement, the lattice constant and band gap of the InGaAs QWR could be estimated using Vegard's law. The uneven distribution of indium and gallium atoms resulted in the fluctuation of the lattice constant, with a larger lattice constant at the bottom and a smaller lattice constant at the top of the QWR. The variation of the lattice constant further complicates the strain distribution in the QWR. For the bottom part of the QWR, we would expect compressive strain from the subjacent InP and the top part of the QWR. While, for the top part of the QWR, we would expect tensile strain from the upper InP and the bottom part of the QWR. The composition fluctuation also leads to variation of band gap. The bottom part of the QWR with a higher indium composition has a smaller band gap, while the top part with a higher gallium composition has a larger band gap. The actual energy difference between different parts of the QWR should be even larger due to strain-induced band splitting and difference in quantum confinement.

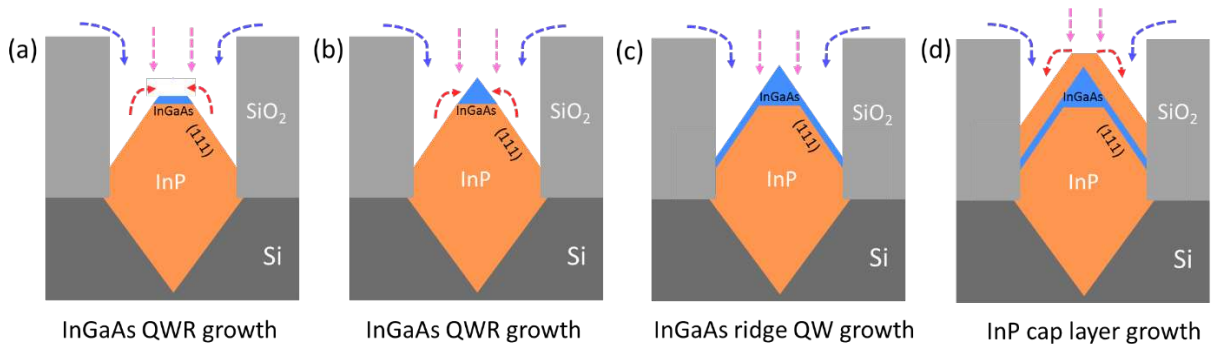


Figure 4. Schematics showing the mechanism of QWR formation when the self-limiting shape of InP exceeds that of InGaAs. Pink dotted lines indicate the direct supply of adatoms from the reactor; blue dotted lines show the diffusion of adatoms from the oxide mask to the trench; Red lines refer to the inter-facet diffusion of adatoms. (a) The selective growth of InGaAs at the InP tip; (b) The formation of triangle-shaped InGaAs QWR; (c) Continued growth leads to the formation of InGaAs ridge QW; (d) The growth of InP cap layer towards the self-limiting growth profile.

Based on the TEM investigation of InGaAs QWRs with varied growth time, we schematically summarized the growth mechanism of InGaAs QWRs inside InP nano-ridge in figure 4. For III-V materials grown inside nano-scale trenches, a self-limiting growth profile, with a fixed size of convex {111} facets and top (001) facet (sometimes surrounded by transitional facets), is developed to minimize the total surface energy during the SAG process.²⁴ The width of the top (001) facet is determined by the surface energy of different facets and the interfacial energy with the SiO₂ sidewall, which could be tuned by varying the growth conditions.²⁵ The formation of InGaAs QWRs instead of ridge QWs lies in the premise that the self-limiting size of (001) facet of InGaAs is smaller than that of InP. As shown in figure 4(a) and (b), the initial epitaxy of InGaAs on InP exhibits a huge growth preference along the vertical [001] direction to minimize the (001) facet, and InGaAs QWR is formed in this phase. After InGaAs reaches its self-limiting shape, further deposition leads to the growth on {111} facets and thereby the formation of ridge QWs (figure 4(c)). The width (i.e. along $[1\bar{1}0]$ direction) of the InGaAs QWR structure is directly inherited from the size of (001) facet of the underneath InP ridge, while the vertical dimension ([001] direction) could be tuned by simply varying the growth time. The InP cap layer deposited directly after the InGaAs layer would reach the self-limiting shape after a certain thickness (figure 4(d)).

One challenge of III-V hetero-epitaxy on Si is the generation of defects due to lattice and thermal mismatches. Minimizing the impairment of the crystalline imperfections on the gain medium is essential for high performance light emitters directly grown on Si. As an example, figure 5(a) shows the cross sectional TEM image of one InP nano-ridge with an InGaAs QWR growth time of 15 sec. While, most of the defects (dark area at the III-V/Si interface) are confined within the V-grooved pocket, the InP buffer outside the V-grooved pocket exhibits good crystalline

quality. One stacking fault (SF), originating at the InP/Si interface, propagates upwards, penetrates the bottom quasi-QWR and reaches the top (111) InP surface. Despite intrusion into the InP buffer layer, planar defects on {111} planes parallel to the trench direction could not propagate into the top three QWRs and would terminate at the {111} B InP facets or the SiO₂ sidewall. While (1 $\bar{1}$ 1)/($\bar{1}$ 11) planar defects and inclined threading dislocations could be completely trapped, (111)/($\bar{1}\bar{1}$ 1) planar defects perpendicular to the trench direction could not be blocked, as illustrated by the schematic depicted in figure 5(c). We found that the (111)/($\bar{1}\bar{1}$ 1) planar defects could be revealed by selective wet etching (H₂SO₄:H₂O₂:H₂O = 1:1:10). Figure 5(b) highlights the (111)/($\bar{1}\bar{1}$ 1) planar defects terminated at the InP surfaces. The density of these planar defects is calculated to be around 1.0/micron. Because of the small dimension and high position, the possibility of the top three QWRs being penetrated by dislocations is greatly reduced. In fact, the top three QWRs are immune to the influence of the most common 60° dislocations gliding along the {111} planes (see figure 5(c)).

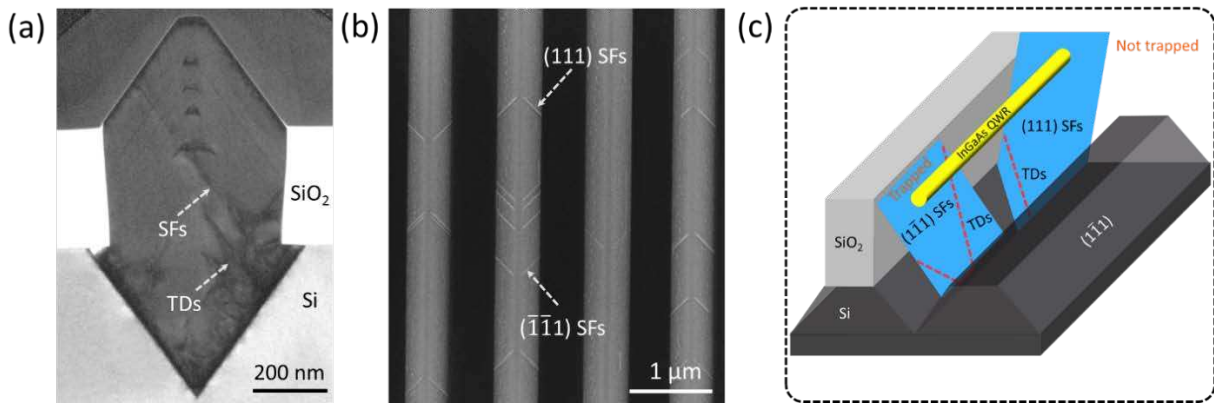


Figure 5. (a) Cross-sectional TEM image (perpendicular to the trench direction) of a single InP nano-ridge, indicating the confinement of defects inside the V-grooved pocket; (b) Top-view SEM image of InP nano-ridge array with exposed {111} planar defects perpendicular to the trench direction; (c) Schematic showing the defect trapping mechanism of ART and the immunity to stacking faults and dislocations of the QWRs.

The minimized influence of defects is manifested by the outstanding optical property of the InGaAs QWRs at telecom-bands as revealed by room-temperature μ -PL measurements. The excitation from a 1064 nm continuous-wave laser was focused to a line-shaped spot ($40 \mu\text{m} \times 4 \mu\text{m}$), and PL from the sample was harvested by a thermoelectric-cooled InGaAs detector through the same objective. The normalized PL spectra of the InGaAs QWRs with 15 sec growth time is displayed in figure 6(a). With a relatively low excitation density of 1.10 kW/cm^2 , the main peak resides around 1600 nm with light emission coming from the InGaAs QWRs. A smaller bump at 1340 nm corresponds to light emission of the ridge QWs. As the laser power density was increased to 21.5 kW/cm^2 , the main peak shifted to 1550 nm by band-filling effects, and the peak at 1340 nm strengthened due to increasing number of escaped photo-generated carriers from the QWRs to the ridge QWs. However, the sudden decrease of the PL intensity beyond 1600 nm is due to the cutoff of the InGaAs detector at long wavelengths. Figure 6(b) displays the PL spectra of QWRs with 2.0 sec growth time under increasing excitation power density. The single-peak characteristic at all excitation levels indicates that light emission comes solely from the QWRs. The broadening of the emission spectra under high excitation level could be attributed to the composition inhomogeneity and band-filling effects. Normalized PL spectra of QWRs with different sizes is presented in figure 6(c), suggesting the blue-shift of emission peak with reducing wire size. Notably, by simply tuning the growth time of the QWRs, the emission spectrum could cover the whole telecommunication bands.

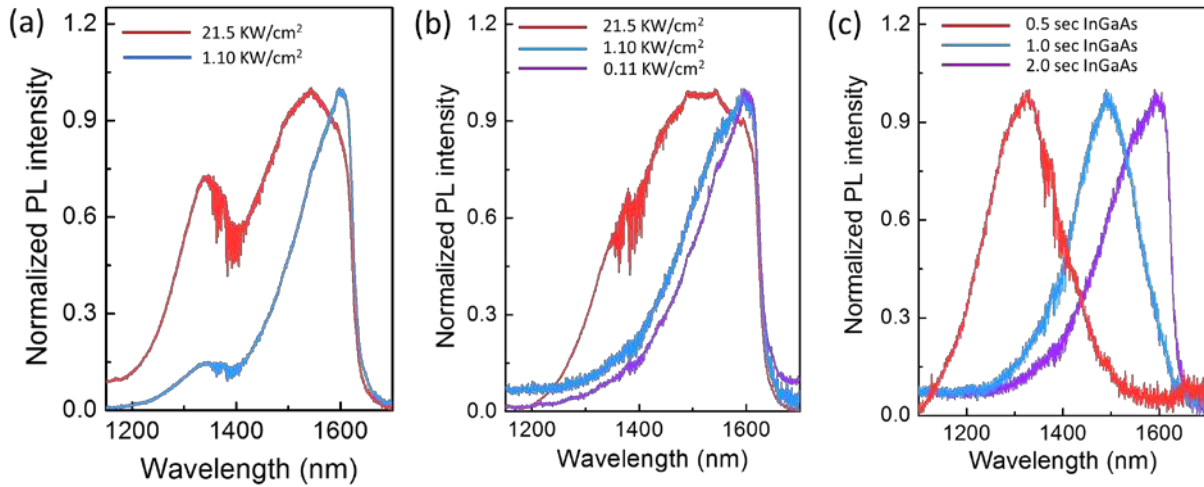


Figure 6. (a) Room temperature μ -PL spectra of the InGaAs QWRs with a 15 sec growth time under different excitation levels; The peak at 1500 nm band comes from the QWRs and the peak at 1300 nm band comes from the ridge InGaAs QWs. (b) Room temperature μ -PL spectra of the InGaAs QWRs with a 2.0 sec growth time under different pumping power densities. Single-peaked characteristic suggests light emission from the QWRs; (c) Room temperature μ -PL spectra of InGaAs QWRs with different growth time under 1.10 kW/cm², indicating the blue-shift of emission peak with reducing growth time. Notably, light emission from the three QWRs covers the whole telecom bands.

Conclusion

In conclusion, we have demonstrated the growth of multi-InGaAs QWRs inside InP nano-ridge arrays on mainstream (001) Si substrates emitting at telecom wavelengths. We also present a comprehensive study of the mechanism of QWR formation via extensive TEM investigation at different growth stages. The insertion of low dimensional quantum structures with modified DOS inside an III-V nano-ridge array shows promises in development of high performance nano-lasers and high density optical links directly grown on Si.

Acknowledgements

This work was supported in part by Grants (Nos. 16245216 and 16212115) from the Research Grants Council of Hong Kong and in part by the Innovation Technology Fund of Hong Kong (No. ITS/273/16FP). The authors would like to thank the MCPF and NFF of HKUST for technical support. Helpful discussions with C. W. Tang and B. Shi are also acknowledged.

References

- [1] Z.P Zhou, B. Yin, and J. Michel, *Light: Science & Applications*. **2015**, 4(11), 358.
- [2] D. Lang and J. E. Bowers, *Nature Photonics*. **2010**, 4, 511.
- [3] A. L. Liu, C. Zhang, J. Norman, A. Snyder, D. Lubyshev, J. M. Fastenau, A. W. K. Liu, A. C. Gossard, and J. E. Bowers, *Appl. Phys. Lett.* **2014**, 104, 041104.
- [4] S.M. Chen, W. Li, Wu. J, Q, M.C. Tang, S. Shutts, S.N. Elliott, A. Sobiesierski, A.J. Seeds, I. Ross, P.M. Smowton, and H.Y. Liu, *Nat. Photonics* **2016**, 10, 307-311.
- [5] Y. Wan, Q. Li, A. Y. Liu, A. C. Gossard, J. E. Bowers, E. L. Hu, K. M. Lau, *Optics Letters*. **2016**, 41 (7), 1664.
- [6] B. Shi, S. Zhu, Q. Li, C.W Tang, Y.T. Wan, E.L. Hu, and K.M. Lau. *Appl. Phys. Lett.* **2017**, 110, 121109.
- [7] J. Z. Li, J. Bai, J-S. Park, B. Adekore, K. Fox, M. Carroll, A. Lochtefeld, and Z. Shellenbarger, *Appl. Phys. Lett.* **2007**, 91, 021114.
- [8] W. Guo, L. Date, V. Pena, X. Bao, C. Merckling, N. Waldron, N. Collaert, M. Caymax, E. Sanchez, E. Vancoille, K. Barla, A. Thean, P. Eyben, and W. Vandervorst, *Appl. Phys. Lett.* **2014**, 105, 062101.
- [9] M. Paladugu, C. Merckling, R. Loo, O. Richard, H. Bender, J. Dekoster, W. Vandervorst, M. Caymax, and M. Heyns, *Cryst. Growth Des.* **2012**, 12(10), 4696.
- [10] C. Merckling, N. Waldron, S. Jiang, W. Guo, N. Collaert, M. Caymax, E. Vancoille, K. Barla, A. Thean, M. Heyns, and W. Vandervorst, *J. Appl. Phys.* **2014**, 115, 023710.

- [11] T. Orzali, A. Vert, B. O'Brian, J.L. Herman, S. Vivekanand, S. S. P. Rao, and S. R. Oktyabrsky, *J. Appl. Phys.* **2016**, 120, 085308.
- [12] Z. Wang, B. Tian, M. Paladugu, M. Pantouvaki, N. Le Thomas, C. Merckling, W. Guo, J. Dekoster, J. Van Campenhout, P. Absil, and D. Van Thourhout, *Nano Lett.* **2013**, 13, 5063.
- [13] Z.C Wang, B. Tian, M. Pantouvaki, W.M Guo, P. Absil, J.V. Campenhout, C. Merckling, and D. V. Thourhout, *Nat. Photonics.* **2015**, 9(12), 837-842.
- [14] Qiang Li, Billy Lai, and Kei May Lau. *Applied Physics Letters.* **2017**, 111 (17), 172103.
- [15] B. Kunert, W. Guo, Y. Mols, B. Tian, Z. Wang, Y. Shi, D. Van Thourhout, M. Pantouvaki, J. Van Campenhout, R. Langer, and K. Barla, *Appl. Phys. Lett.* **2016**, 109, 091101.
- [16] B. Tian, Z. Wang, M. Pantouvaki, P. Absil, J. Van Campenhout, C. Merckling, and D. Van Thourhout, "Room temperature O-band DFB laser array directly grown on (001) silicon," *Nano Lett.* 17(1), **2017**, 559–564.
- [17] R. Cipro , T. Baron , M. Martin , J. Moeyaert , S. David , V. Gorbenko , F. Bassani , Y. Bogumilowicz , J. P. Barnes , N. Rochat , V. Loup , C. Vizioz , N. Allouti , N. Chauvin , X. Y. Bao , Z. Ye , J. B. Pin , and E. Sanchez , *Appl. Phys. Lett.* **2014**, **104**, 262103.
- [18] Q. Li, Y. Han, X. Lu, and K.M Lau, *IEEE Electron Device Lett.* 37, 24-27.
- [19] S. Li, and X. Zhou, and M. Li, and X. Kong, and J. Mi, and M. Wang, and W. Wang, and J. Pan, *Appl. Phys. Lett.* **2016**, 108, 021902.
- [20] L. Megalini, B. Bonef, B.C. Cabinian, H.W Zhao, A. Taylor, J.S. Speck, J.E. Bowers, and J. Klamkin. *Appl. Phys. Lett.* **2017**, 111(3), 032105.

- [21] Yu Han, Qiang Li, Si Zhu, Kar Wei Ng, and Kei May Lau. Applied Physics Letters. **2017**, 111(21), 212101.
- [22] Y. Han, Q. Li, S.P. Chang, W.D. Hsu, and K.M. Lau, Appl. Phys. Lett. **2016**, 108, 242105.
- [23] Y. Han, Q. Li, and K.M. Lau, J. Appl. Phys. **2016**,120, 245701.
- [24] G. Biasiol, A. Gustafsson, K. Leifer, and E. Kapon, Phys. Rev. B. **2002**, 65, 205306.
- [25] S. Jiang, C. Merckling, W. Guo, and N. Waldron, J. Appl. Phys. **2014**,115, 023517.